Research paper

Mixed matrix hollow fibre membrane comprising polyetherimide and modified montmorillonite with improved filler dispersion and CO_2/CH_4 separation performance

Asif Jamil, Oh Pei Ching *, Azmi M. Shariff

Department of Chemical Engineering, Universiti Teknologi PETRONAS, Bandar Seri Iskandar 32610, Perak, Malaysia

ABSTRACT

Mixed matrix membrane with nano-filler embedded in polymer matrix, is receiving overwhelming attention for gas separation applications due to its attractiveness in providing an economic solution to enhance permselectivity. However, achieving uniform dispersion of nano-filler in host polymer remains a key challenge in developing membrane. In this work, mixed matrix hollow fibre membranes comprising polyetherimide (PEI) with various modified montmorillonite (*f*-Mt) loading, was developed via phase inversion method for CO_2/CH_4 separation. The Mt was modified with aminolauric acid to impart organophilicity to enhance compatibility towards organic polymer matrix. The synthesized hollow fibers were characterized using field emission scanning electron microscopy (FESEM), energy dispersive X-ray spectroscopy (EDX), thermal gravimetric analysis (TGA), differential scanning calorimetry (DSC), and permeation test. The permeation tests were carried out with pure gases at ambient temperature with varying pressures of 2 and 4 bars. An increasing trend in ideal selectivity was observed up to 2 wt% *f*-Mt loading. Thereafter, opposite trend was observed with increasing filler loading due to exfoliated layers that created more tortuous path for the penetrating gas molecules. The maximum ideal selectivity was found with 2 wt% *f*-Mt loading at 2 bar, which showed 39% increment as compared to neat PEI hollow fibre membrane. This increment in gas selectivity was related to the dispersion state and aspect ratio of *f*-Mt. Various phenomenological models were employed to calculate the aforementioned properties. Adopting to Cussler and Yang-Cussler models, the aspect ratio of the *f*-Mt was found to be 35 and 50, respectively with 3–4 particles per tactoid.

© 2017 Elsevier B.V. All rights reserved.

1. Introduction

Mixed matrix membrane (MMM) has gained significant attention in virtue of its superior transport properties, ease in processing and low cost. Robust and efficient material selection could enhance its viability for industrial scale gas separation application. Generally, the synergistic advantages of both organic and inorganic phases in MMM lead it to surpass the upper bound performance curve which could not be achieved with neat polymer membranes (Jamil et al., 2016a, 2016b). However, the selection criteria of appropriate materials is often complicated, in which several parameters such as compatibility, durability, productivity and mechanical properties should be considered (Chung et al., 2007). In fact, poor materials selection could lead to insufficient interfacial interactions that deteriorate the selective gas transport properties of membrane. Nano-sized inorganic fillers offer high gas separation performance due to their ability to improve interface interactions

towards organic phase, as well as to interact with gas molecules (Rubio et al., 2014). Therefore, suitable nano-filler selection for polymer phase will result in improved mechanical strength, defect-free structure that can withstand robust conditions without compromising the separation performance (Iman et al., 2014). Thus far, zeolites and molecular sieves are widely used nanofillers for MMM development. In recent years, many other novel materials like carbon nanotubes (CNT), graphene, clay minerals and metallic organic frameworks (MOF) have been adopted to enhance MMM properties beyond that of the polymer matrix (Kim et al., 2005; Goh et al., 2011; Jamil et al., 2014).

Montmorillonite (Mt), a type of clay mineral generally used in clay-polymer composites (CPN), has yet to gain much attention in MMM fabrication despite its tremendous nanofiller potential (Mittal, 2009). In the 1990s, Mt finds application as reinforcing filler in the automotive industry and is extensively used to this day. The Toyota research group emerged as pioneer in this regard, successfully commercializing nylon-6-Mt nanocomposite. According to their findings, with a small addition of Mt (4.2 wt%), the modulus and tensile strength increased by 50% (Jamil et al., 2016a, 2016b). Since then, researchers have

* Corresponding author.
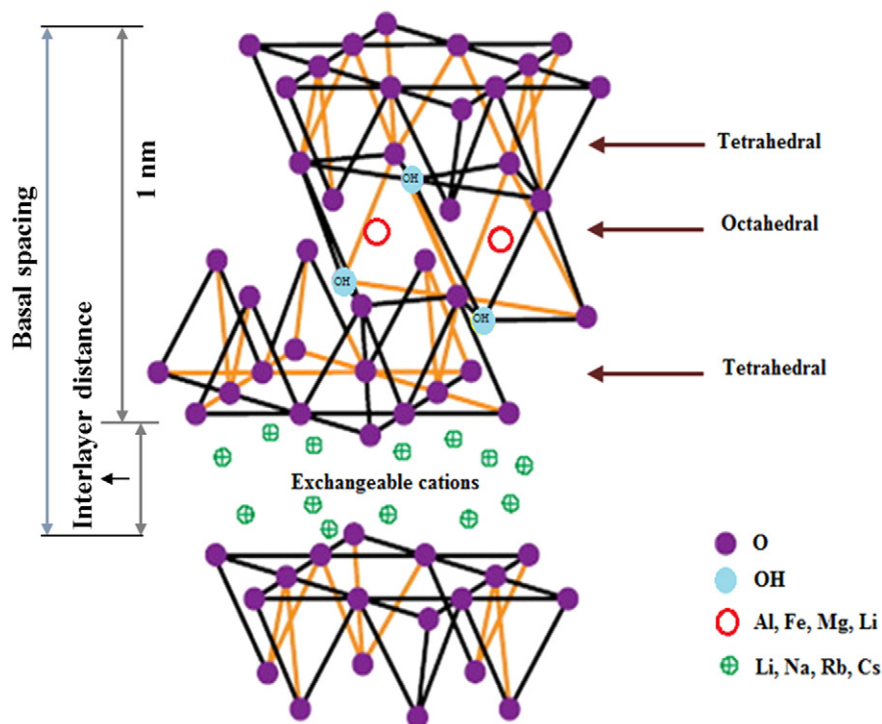 *E-mail address:* peiching.oh@utp.edu.my (O.P. Ching).

Fig. 1. Structure of 2:1 phyllosilicates (Pavlidou and Papaspyrides, 2008).

thoroughly investigated Mt application in thermoplastic nanocomposites due to their superior mechanical, barrier, thermal, flame-retardant, and abrasive properties (Adame and Beall, 2009; Anadão et al., 2010). Mt is a 2:1 phyllosilictae (Fig. 1) and its elementary structural unit contains a tetrahedral layer composed of silicon surrounded by four oxygen atoms, and octahedral sheet which contains aluminum encircled by eight oxygen atoms (Uddin, 2008). The thickness of each layer is 1 nm and the lateral dimension is 300 Å to several micrometer with an aspect ratio of over 1000 (Jamil et al., 2016a, 2016b). Mt possesses relatively weak interlayer van der Waals forces as a result of the interlayer distance which depends on the type of cation present in between the layers. Moreover, the particles of Mt are held together by electrostatic forces, in which the negatively charged layers attract water molecules and inorganic cations. The exchangeable cations are not structurally bonded to Mt (weakly bonded), thus can be easily replaced with other positively charged cations. Besides that, the pristine form of Mt is hydrophilic and miscible with hydrophilic polymers like poly(ethylene oxide) and poly(vinyl alcohol). In order to render miscibility towards hydrophobic polymers, the inorganic cations present in Mt must be exchanged with organic cations (Pavlidou and Papaspyrides, 2008).

The replacement of inorganic to organic cations in Mt can be performed either by covalent or non-covalent interactions. The former interactions are governed by condensation, silylation and esterification reactions, whereas the latter are driven by cation exchange, van der Waals interactions, dipole-dipole interactions and acid-base interactions. Covalent modification provides good control on the interactions of modifying agents and clay mineral surfaces, however, the basic structure of clay mineral has changed during such interactions (Takahashi and Kuroda, 2011). Generally, organic cations improve the wetting with polymer by lowering the surface energy of the Mt (Mittal, 2009). Conventionally, alkylammonium ions are mostly used along with other organic cations like sulfonium and phosphonium (Zanetti et al., 2000). For some cases, alkylamonium cations can provide functional groups that initiate polymerization of monomers. Furthermore, the alkylamonium cations attach to the surface of negatively charged Mt layers and its long organic chains increase the interlayer distance (Kim

et al., 2001). Okada and Usuki (1995) who modified Na-Mt with ammonium cations containing 18 carbon atoms in the main chain observed that the modified Mt has increased interlayer distance from 1.27 nm to 2.82 nm. In addition, the lengthy alkyl chains impart organophilicity in Mt, thereby improve its mixing and interfacial interactions with the polymer matrix (Nassar et al., 2005). On top of that, the expansion of Mt layers assist polymer chains to migrate in the interlayer space that benefits the two phase interfacial interactions and uniform dispersion of inorganic filler in polymer matrix (Pavlidou and Papaspyrides, 2008).

The dispersion state of inorganic fillers is defined by the tortuosity factor that affects the permeation properties of the diffusing gas molecules. Various phenomenological models have been developed to define the tortuous effect based on the geometrical structure and volume fraction of the clay mineral particles (Picard et al., 2007). To date, every model considered polymer as the permeable whereas clay mineral was deemed as the impermeable phase. Besides that, the models are developed based on the assumption of fully exfoliated layers, therefore the predictor models become less effective when exfoliating and delaminating phases exist simultaneously in MMM. Delamination of the silicate represents the intercalation of polymer chain in interlayer space whereas exfoliation describes the complete separation of the layers which is required to enhance the membrane properties even at lower loading. In general, the dispersion state of layered silicates are either estimated by TEM analysis or calculated through theoretical modeling (Picard et al., 2007; Tan and Thomas, 2016).

Most studies on clay-polymer MMM used flat sheet membrane configuration despite the various advantages associated with hollow fibre

Table 1
Dope solution composition and viscosity.

Dope solutions	PEI (wt%)	NMP (wt%)	f-Mt (wt% of PEI)	f-Mt vol. fraction (Φ)	Viscosity (cp)
Neat PEI	23	77	0	0.000	5617
PEI-f-Mt(1)	23	77	1	0.005	10,993
PEI-f-Mt(2)	23	77	2	0.010	14,457
PEI-f-Mt(3)	23	77	3	0.014	16,115
PEI-f-Mt(4)	23	77	4	0.019	18,456

Table 2
PEI-*f*-Mt hollow fibre membrane spinning parameters.

Spinning conditions	Dope solution
OD/ID (mm)	0.8/0.4
Coagulant	Water
Coagulant temperature (°C)	25
Air gap (cm)	15
Dope solution flow rate (mL/min)	0.8
Bore water flow rate (mL/min)	1
Take up velocity	Free fall

(HF) membrane; the latter has more surface to volume ratio and higher productivity per unit volume (Khayet, 2003). Different polymers have been investigated for synthesis of gas separation membranes, however, several advantages such as superior gas selectivity, chemical stability, thermal stability and ease in spinning made polyetherimide (PEI) a very attractive choice compared to polysulfone and polyethersulfone (Chung et al., 1992; Wang et al., 2002). Even dispersion and compatibility of clay minerals in host polymer are the few fundamental issues that hinders the gas separation application of clay-polymer mixed matrix membranes.

Therefore, the main focus of this study is to investigate the potential of Mt in PEI matrix for development of HF membrane in CO_2/CH_4 separation application. Na-Mt containing Na^+ as interlayer cations are replaced with aminolauric acid with alkyl chain containing twelve carbon atoms through cation exchange to improve organic-inorganic interfacial interactions and dispersion. Experimentally determined CO_2 permeance values are compared with calculated values through various existing models and the dispersion state of *f*-Mt is determined through the models. To the best of our knowledge, no study has been performed on HF membrane embodying modified Mt as inorganic phase and PEI as continuous phase spun through phase inversion technique to improve CO_2/CH_4 separation.

2. Methodology

2.1. Materials

KUNIPIA-F a type of Na-Mt with cation exchange capacity (CEC) of 119 meq/100 g was provided with courtesy by Kunimine Ind. Co., Japan. *N*-methyl-2-pyrrolidone (NMP, 99.5%), 12-aminolauric acid (95%), and polyetherimide (PEI, melt index 9 g/10 min) were purchased from Sigma Aldrich, whereas HCl (37%) was supplied by Merck. PEI was dried at 120 °C overnight prior to use. NMP, HCl and 12-aminolauric acid were used as received. The interlayer modification of Na-Mt was performed as mentioned elsewhere (Okada and Usuki, 1995). For the sake of simplicity, modified-Mt is hereafter denoted as *f*-Mt.

2.2. Modified montmorillonite characterization

2.2.1. X-ray diffraction
Small angle X-ray diffraction analysis (BRUKER, XRD/D8) was used with CoKα radiation (0.15414 nm) to measure the basal spacing of both Mt and *f*-Mt. The XRD measurements were performed over a 2θ
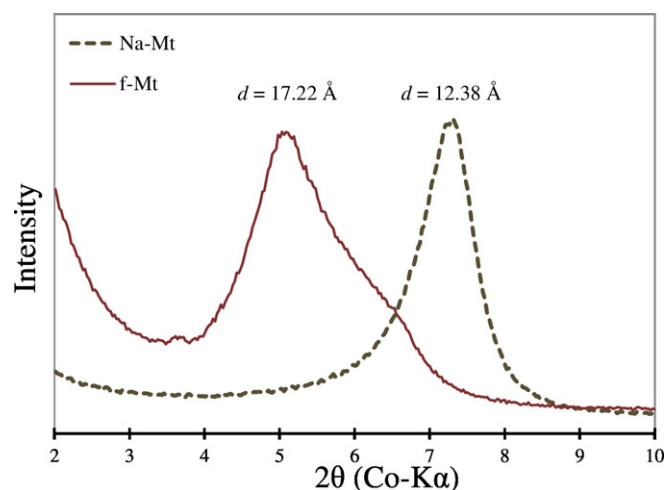

Fig. 2. XRD analysis of Na-Mt and *f*-Mt.

range of 2–10. Bragg's equation ($n\lambda = 2\sin\theta$) was used to measure the basal spacing of Na-Mt and *f*-Mt peaks.

2.2.2. Dispersibility test
The Mt and *f*-Mt samples were dispersed in water and ethanol at room temperature at a concentration of 10 g/L according to the method proposed by Zhou et al. (2009). The dispersed samples were sonicated for 30 min and kept for observation.

2.3. Dope solution preparation

The dope solution for spinning HF membrane consists of 23 wt% PEI and 77 wt% of NMP with varied amount of *f*-Mt (0–4 wt% of PEI). The desired amount of *f*-Mt was dispersed in NMP and sonicated for 60 min at 40 °C for uniform dispersion followed by addition of 10% PEI for priming purpose together with stirring for 3 h at 70 °C. Subsequently, the remaining PEI was added in the solution gradually until complete dissolution. The prepared dope solution was degassed at room temperature for 12 h for complete removal of bubbles formed during stirring. Prior to HF membrane spinning, the viscosity of dope solution was measured by using Fungilab rotational viscometer (Model Alphas L) at 12 rpm (Table 1).

2.4. Fabrication of hollow fibre membrane

HF asymmetric membrane was produced at ambient conditions by phase inversion method using lab-scale HF spinning experimental set up (Table 2). For dope extrusion, tube in orifice spinneret was used with 0.8-mm outer and 0.4-mm inner diameter. The dope solution was pumped to spinneret at constant flow rate and constant N_2 pressure was applied at 1 bar. Bore fluid (flows inside hollow cylindrical area of membrane) water was delivered through syringe pump. Distilled water was used as both internal and external coagulant and air gap distance was fixed at 15 cm at constant relative humidity. The nascent

Table 3
Phenomenological models used to calculate *f*-Mt aspect ratio.

Models	Equation	Ref.	Description
Nielsen	$\frac{P_c}{P_o} = \frac{1-\varphi}{1+\frac{\alpha\varphi}{2}}$	Nielsen, 1967	Where P_c, permeability of composite
Cussler	$\frac{P_c}{P_o} = \left(1 + \frac{\alpha^2\varphi^2}{1-\varphi}\right)^{-1}$	Cussler et al., 1988	P_O, neat polymer membrane permeability φ, filler volume fraction
Yang-Cussler	$\frac{P_c}{P_o} = \frac{1-\varphi}{1+{}^1/_2(\alpha^2\varphi^2)}$	Yang et al., 2004	α, aspect ratio S, is the order factor
Lape-Cussler	$\frac{P_c}{P_o} = \frac{1-\varphi}{[1+({}^2/_3)\alpha\varphi]^2}$	Lape et al., 2004	$S = 0$, random orientation
Bharadwaj	$\frac{P_c}{P_o} = \frac{1-\varphi}{[1+({}^1/_3)\alpha\varphi(S+{}^1/_2)]}$	Bharadwaj, 2001	$S = -1/2$, parallel orientation to the direction of flow $S = 1$, horizontal orientation to the flow direction

Table 4
Dispersibility[a] test of Na-Mt and f-Mt in water and ethanol.

Samples	Water	Ethanol
Na-Mt	++	±
f-Mt	−	++

[a] ++: Better dispersibility, cloudy supernatant but uniform, lower sample is swelling. +: Good dispersibility, cloudy supernatant but non-uniform, lower sample is swelling. ±: Bad dispersibility, clear supernatant, lower sample is swelling. −: Worst dispersibility, clear supernatant, lower sample is not swelling.

spun fibre passed through coagulation bath for solvent exchange and was collected by the take-up drum. Subsequently, the spun hollow fibers were immersed in distilled water for solvent exchange for 3 days with daily water change to remove solvent residues, followed by fibre drying at ambient conditions.

2.5. Pure gas permeation test

Gas permeation test was carried out by using 99.99% pure CO_2 and CH_4 gases at room temperature and at pressure of 2 and 4 bars. A pile containing 20 fibers was injected in the module with one end of pile glued with epoxy resin to avoid gas passage, whereas the other end of the pile was accessible to the desired inlet gases. Permeation was carried out by passing the desired gas through the lumen side of the hollow fibers. The total effective area of the fibers was approximately 106.5 cm². A bubble flow meter was attached to the gas permeate side in order to measure the flow rate of gas through the membrane. The permeance was calculated by using Eq. (1).

$$\frac{P_i}{l} = \frac{Q}{A\Delta P}\frac{273.15}{T}$$
(1)

where P_i/l is the permeance of gas in GPU [1 GPU = $1 * 10^{-6}$ cm³(STP)/cm² s cm Hg]. Subscript, i, represents the penetrating gas, i.e., CO_2 or CH_4. Q (cm³/s), volumetric flow rate, A (cm²), is the effective surface area, ΔP is the pressure difference across membrane in cm Hg and T (K) is the temperature at which permeation was carried out. The ideal

selectivity is the ratio of permeance of fast gas to slow gas and was calculated by using Eq. (2).

$$\alpha_{ij} = \frac{P_i/l}{P_j/l}$$
(2)

α_{ij} represents ideal selectivity of gas i to j. Whereas P_i/l, P_j/l represents permeation of gas i and j, respectively.

2.6. Gas permeation modeling

The transport of gas molecules in layered silicates is a complex phenomenon governed by diffusion/solubility mechanism. Generally, the transportation of gas molecules through polymer phase depends on both the solubility of the penetrant molecules and diffusivity through the polymer surface followed by desorption from the other surface (Cui et al., 2015). The permeation of penetrant molecules can be explained via Fickian diffusion which states that the permeation coefficient depends on both diffusion coefficient and solubility coefficient as given in Eq. 3.

$$P = DS$$
(3)

Diffusion coefficient, D (in m²/s), describes the kinetic properties of penetrant molecules which depends on its mobility in polymer phase whereas solubility coefficient, S (in mol/m³ Pa), the thermodynamic factor which reflect the interactions between organic and inorganic phase (Yampolskii, 2012; Cui et al., 2015).

The tortuosity of the layered silicates plays a major role in permeation reduction and is dependent on three factors; volume fraction, orientation of layers and aspect ratio. With the increase in volume fraction of impermeable phase, volume of available permeable phase for penetrant molecules decreased, therefore, solubility factor and permeability also decrease. The perpendicular orientation of layered silicate to the diffusion path result in decrement of diffusion coefficient of penetrant molecules, whereas, parallel orientation shows opposite behavior. The aspect ratio defined the state of delamination and exfoliation of layered
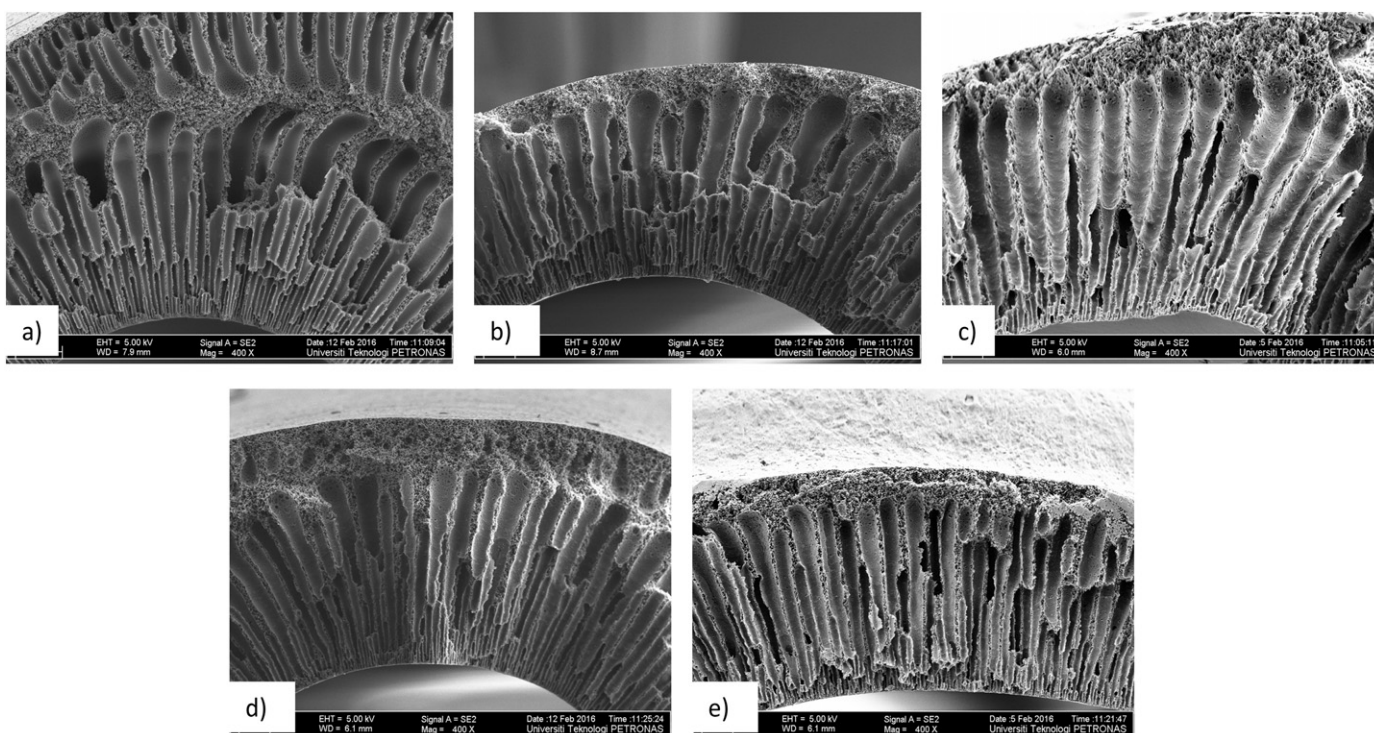

Fig. 3. FESEM images of hollow fibre membranes, a) Nascent PEI, b) PEI-f-Mt(1), c) PEI-f-Mt(2), d) PEI-f-Mt(3), e) PEI-f-Mt(4).

silicate in polymer matrix; higher aspect ratio favors exfoliation and dispersion of individual layer in the polymer matrix which increase the tortuous path for penetrant gas molecules and reduce the permeation. Delamination of layered silicate represents the intercalation of polymer chain in the interlayer space whereas exfoliation represents the complete separation of layers which is required to enhance the membrane properties even at lower loading. However, in most cases, delaminated morphology or mixed morphology of the clay mineral layers are observed rather than complete exfoliation (Choudalakis and Gotsis, 2009).

Several theoretical models are available in literature to predict gas permeation through polymer layered silicates membrane (Table 3). Nielsen (1967) proposed a simple permeation model by considering the regular and horizontal arrangement of layers to the diffusion path. The nanoparticles with rectangular shape are evenly distributed with finite width, L, and thickness, D, in the polymer matrix. Cussler et al. (1988) improved the model by considering the nanoparticles arranged in layered form with each layer separated by narrow slits. This model is more sensitive with regard to aspect ratio and volume fraction for permeability prediction as compared to Nielsen Model. Yang et al. (2004) further improved the model by considering the monodispersed

nanoparticles with parallel alignment and varied aspect ratio. Whereas Lape et al. (2004) considered the rectangular layers with similar aspect ratio are dispersed randomly in polymer matrix and aligned parallel to each other along the diffusion path. All the above stated models are based on the consideration that nanoparticles are aligned horizontally to the penetrant diffusion path. In later years, Bharadwaj (2001) developed model which taken in account the platelet orientation factor. This factor includes various dimensions whether horizontal, parallel or randomly distributed in the direction of the diffusion path. Most models assumed complete exfoliation of nanoparticles, whereas this model described the state of delamination and complete exfoliation.

3. Results and discussion

3.1. Modified montmorillonite

The interlayer distance of Mt which promotes dispersion in PEI matrix was measured by using X-ray diffraction (Fig. 2). The basal spacing of Na-Mt calculated by Bragg's equation was 12.38 Å, which is consistent with the reported value of 12.397 Å (Zhou et al., 2009). The
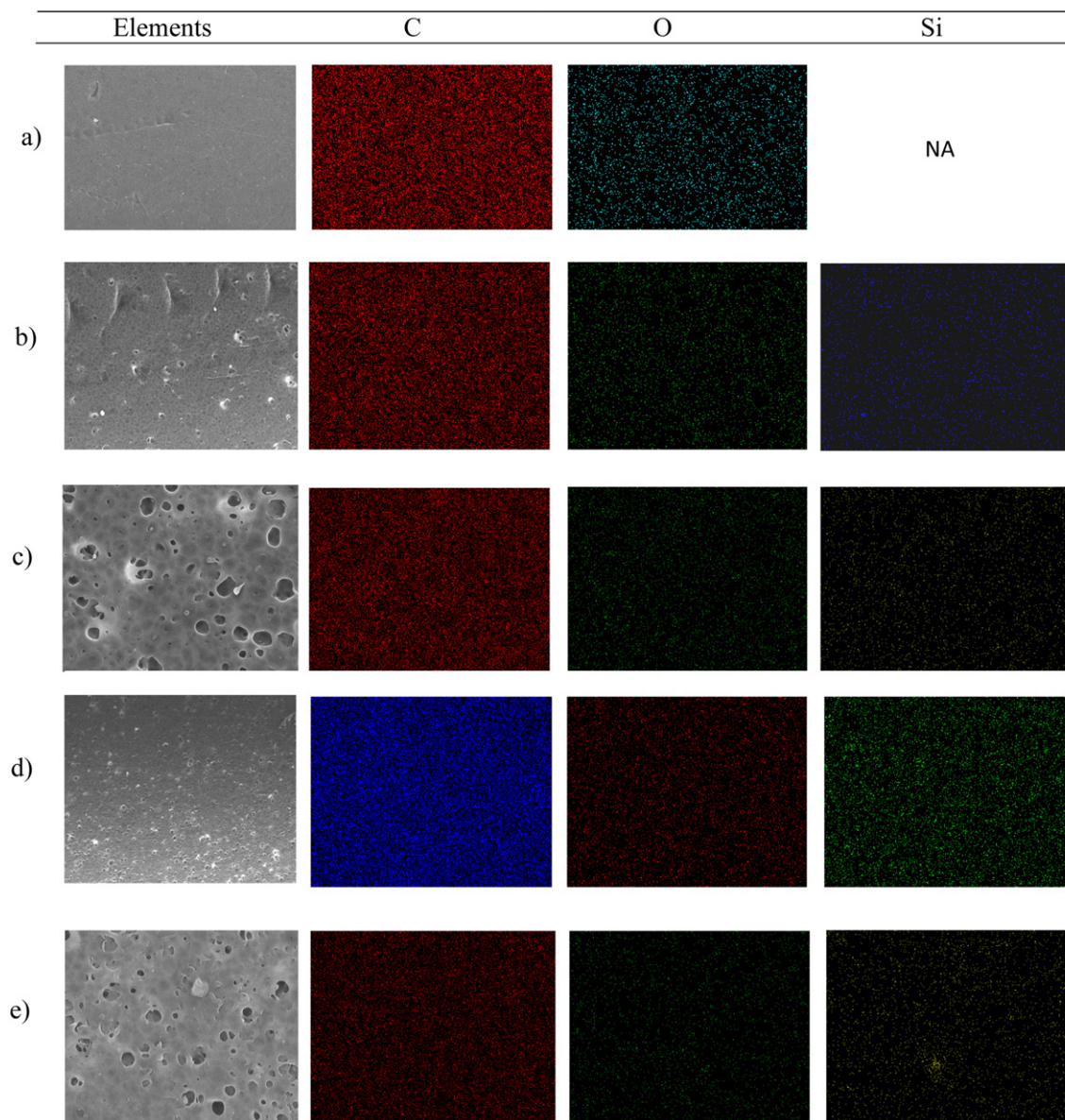

Fig. 4. EDX mapping of C, O, Si elements in PEI-*f*-Mt hollow fibre membrane outer surface, a) Nascent PEI, b) PEI-*f*-Mt(1), c) PEI-*f*-Mt(2), d) PEI-*f*-Mt(3), e) PEI-*f*-Mt(4).

Table 5
EDX elemental analysis of C, O, Si atoms at the outer surface of PEI-f-Mt hollow fibre membrane.

Elements	Neat PEI		PEI-f-Mt(1)		PEI-f-Mt(2)		PEI-f-Mt(3)		PEI-f-Mt(4)	
	wt (%)	at (%)	wt (%)	at (%)	wt (%)	at (%)	wt (%)	at (%)	wt (%)	at (%)
C K	78.63	83.06	78.93	83.42	78.15	82.86	76.74	81.77	77.40	82.55
O K	21.37	16.94	20.65	16.38	21.11	16.80	22.18	17.74	20.70	16.58
Si K			0.43	0.19	0.74	0.34	1.07	0.49	1.90	0.87
Totals	100.00		100.00		100.00		100.00		100.00	

interaction between 12-aminolauric acid and Na-Mt gave lower 2θ value for f-Mt (17.22 Å), implying that the basal spacing of f-Mt has expanded. Okada and Usuki (1995) who modified Na-Mt with the same organic cation also reported basal spacing as 17.2 Å, which further emphasize on the effectiveness of 12-aminolauric in increasing the basal spacing.

Table 4 presents the observations made by dispersing Na-Mt and f-Mt in various solvents. The hydrophilic nature of Na-Mt made it well dispersed in water; however it showed demixing when mixed with ethanol. Zhou et al. (2009) reported similar observation when dispersing Na-Mt in water and ethanol. These observations imply that the Na-Mt is hydrophilic and. In contrast, f-Mt exhibits an opposite behavior in both water and ethanol. It showed worst dispersibility in water, however, relatively good dispersion is observed in ethanol. This is mainly due to the long alkyl chains associated with alkylamonium cations increases the f-Mt's affinity for organic solvents. The dispersibility analysis depicts the hydrophobic nature of f-Mt which made it suitable for uniform dispersion in hydrophobic PEI matrix.

3.2. PEI-f-Mt hollow fibre membrane

The membrane morphology and mechanical properties are governed by phase inversion method. The thermodynamic and kinetic principles involved in phase inversion technique such as polymer-solvent interactions, solvent-coagulant interactions and the dope viscosity affect membrane morphology (Ismail et al., 2015). With the increase in dope solution viscosity, non-solvent diffusion rate in polymer matrix will reduce, therefore the overall membrane forming process is slowed which resulted in irregular pores structure and thick outer skin formation (Rezaei et al., 2014). Depending on the solvent/non-solvent interactions, various types of pores are created i.e. finger-like or sponge-like. The former are created as a result of instant solvent exchange with low molecular orientations whereas the latter are produced with slow exchange of solvent at higher chain orientations. The length of these pores varies from few nanometers to tens of micrometer (Jamil et al., 2016a, 2016b). Finger-like pores promote gas permeance; however, if the pore size is too large, it will result in weak mechanical strength of HF membrane. Sponge-like fibers are helpful in producing highly selective membrane with good mechanical properties (Ren et al., 2004; Husain and Koros, 2009). The pore formation continues until membrane surface touches the external coagulant which solidifies the structure and form dense outer skin layer.

The lower dope solution viscosity along with hydrophobicity, resulted in instant solvent exchange during spinning. As a result, finger-like pores dominate in PEI-f-Mt HF membranes (Fig. 3). All membranes consisted of thin outer skin layer and porous sub-layer. The thin outer skin layer is crucial in determining gas separation performance, whereas the inner layer only acts as the substrate. For all f-Mt concentrations, the outer skin layer obtained was uniform, whereas the inner sub-layers consisted of longer finger-like pores throughout the periphery of the membrane. These long finger like pores were formed due to instant demixing of PEI and NMP. Water molecules diffused from the inner wall of spun HF, whilst NMP solvent migrated to the coagulant liquid. Also, no large Mt particles are observed from the micrographs. This suggests that f-Mt particles were dispersed uniformly throughout the matrix due to vigorous sonication of dope solution and organic modification of Mt particles (DashtArzhandi et al., 2015). The presence of long alkyl group in between the layers weaken the van der Waals interaction, thus, layered exfoliation took place during sonication.

Generally, the dispersion of filler in any polymer phase is a major concern that lowers the membrane separation performance. The energy dispersive X-ray spectroscopy (EDX) mapping (Fig. 4) shows that distribution of Si elements on the membrane outer surface was uniform. The weight percentage of Si increased gradually from nascent PEI HF membrane to 4 wt% f-Mt due to the increased f-Mt loading. The concentration of f-Mt increased from inner to outer surface because during dry wet phase inversion method, elongation of the fibre took place. The fibre front moved inward and may facilitate the incompressible dope solvent to move outward which resulted in f-Mt migration to the outer layer (Zulhairun and Ismail, 2014). The presence of f-Mt at the outer thin skin layer increases the gas selectivity due to the selective properties of clay minerals towards the desired gas. A uniform trend of Si wt% is observed with increasing f-Mt concentration in PEI-f-Mt HF membranes (Table 5). The atomic and weight percent of Si increased gradually at the outer skin layer of spun HF membrane. For 4 wt% of f-Mt, small agglomeration was observed, but the overall distribution was uniform across the rest of the surface.

The thermal properties of spun HF membranes were studied using TGA and DSC. All fibers exhibited single major mass loss in the decomposition curve (Fig. 5). The onset temperature for neat PEI HF
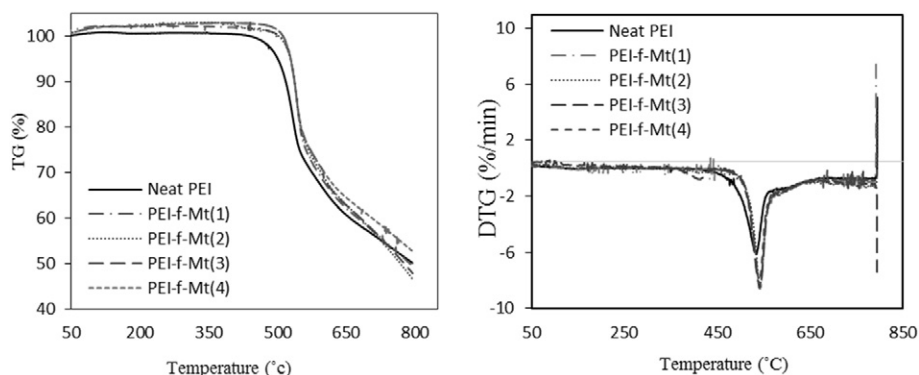

Fig. 5. Thermal decomposition curve of spun hollow fibre membranes.

membrane was approximately 438.16 °C whereas for other compositions of *f*-Mt, the mass loss was approximately 483.26 °C. The +45 °C shift in degradation temperature implies that the thermal properties of hybrid membranes were enhanced. This increase in thermal stability resulted from the inherently good thermal properties of Mt (Jiang et al., 2005). The Mt generated an insulating layer at the polymer surface which hindered the decomposition of more volatile compounds at polymer decomposition stage. The shift of degradation temperature showed good interaction between *f*-Mt and PEI matrix (Liang et al., 2012). However with increasing *f*-Mt loading, no significant improvement in decomposition temperature was observed. It is possible that at high loading, clay mineral acted as catalyst and formed active sites for degradation of polymer (Herrera-Alonso et al., 2010). At low loading, the insulating properties were prominent whereas at higher loading catalytic behavior was dominating.

With the addition of *f*-Mt, the *Tg* reduced gradually (Table 6), signifying an increment in the amorphous phase of PEI-*f*-Mt MMM. Hsiao et al. (2001) found similar decreasing trend in polyimide-clay mineral hybrid film, and speculated that the dodecyl groups in organophilic clay minerals provided significant plasticization effect, thus resulting in reduction of glass transition temperature. This reduction in *Tg* is significant in Mt hybrids film due to its better dispersion (Garg et al., 2011). The dispersed Mt particles hindered the polymer chain orientation as a result crystalline phase decreased.

3.3. Gas separation performance

CO_2 permeance of the hollow fibre membranes was performed at 2 and 4 bar (Fig. 6). Initially, an increasing trend was observed for 1 wt% for *f*-Mt incorporation which decreased above that wt%. This upward and downward trend is supported by Hashemifard et al. (2011) and Zulhairun et al. (2014). Greater chain perturbed orientations, Knudsen diffusion or absence of polymer chain intercalation at interlayer space of clay mineral are the common issues that resulted in lowering the polymer clay mineral interfacial interactions and accelerated the transport of gases through the membrane (Hashemifard et al., 2011). However, unlike aforementioned trend, the opposite behavior was observed in MMM by the addition of clay mineral in polymer matrix. This phenomenon is governed by the organization of clay mineral layers; fully exfoliated form gave rise to the interfacial interactions towards host polymer matrix and tortuous path for the gas to pass through. The tortuous path increased diffusion path length which led to reduction in permeability (Herrera-Alonso et al., 2009; Zulhairun et al., 2014).

The exfoliated layer structure at 1 wt% *f*-Mt in PEI matrix created tortuous path and an increment of 31% and 19% was observed for the ideal selectivity at 2 and 4 bar pressure, respectively (Fig. 6). However, there was limited increase for 3 wt% *f*-Mt in CO_2 permeability because the amino group present at the surface of the layers has affinity for CO_2 gas molecules. Moreover, the highest values of ideal selectivity were approximately 39 and 25 for gas pressures of 2 and 4 bars at 2 wt% *f*-Mt loading. At this loading, gas molecules encountered more obstacles induced by extended tortuous path as compared to 1 wt% *f*-Mt loading.

Compared to neat PEI membranes, the permeance decreased for 3 wt% loading whereas selectivity was higher. This phenomenon is attributed to the intercalated phase's interlayer space which was packed with PEI chains and distributed throughout the host polymer, ultimately increased tortuous path for both gases; this could also be caused due to *f*-Mt was well distributed in the polymer phase. However, with further increase in filler loading, the *f*-Mt particles tend to form agglomerates which led to phase separated distribution. The long alkyl chains at the Mt surface suppressed the void morphology. As a result, both permeability and selectivity decreased at 2 bar pressure. However, at 4 bar, the phase separated morphology took place as a sudden increase in CO_2 permeance was observed.

Table 6
Glass transition temperature of spun membranes.

Sample	*Tg* (°C)
Neat PEI	211.73 ± 0.01
PEI-*f*-Mt(1)	209.81 ± 0.01
PEI-*f*-Mt(2)	209.09 ± 0.01
PEI-*f*-Mt(3)	209.08 ± 0.01
PEI-*f*-Mt(4)	208.74 ± 0.01

3.4. Modeling and discussion

The permeation properties of polymer-layered silicates MMM are strongly dependent on organic-inorganic phase interaction, the dispersion state, aspect ratio and the length of the inorganic particles. In this study, different phenomenological models were used to study the permeation properties of PEI-*f*-Mt MMM, and to determine the dispersion state of the dispersed *f*-Mt in PEI matrix. Theoretical permeation curves were generated (Fig. 7) from Nielsen, Cussler, Yang-Cussler, Lape-Cussler and Bharadwaj models. The relative permeation curves generated through all the models shows a decreasing trend by increasing the
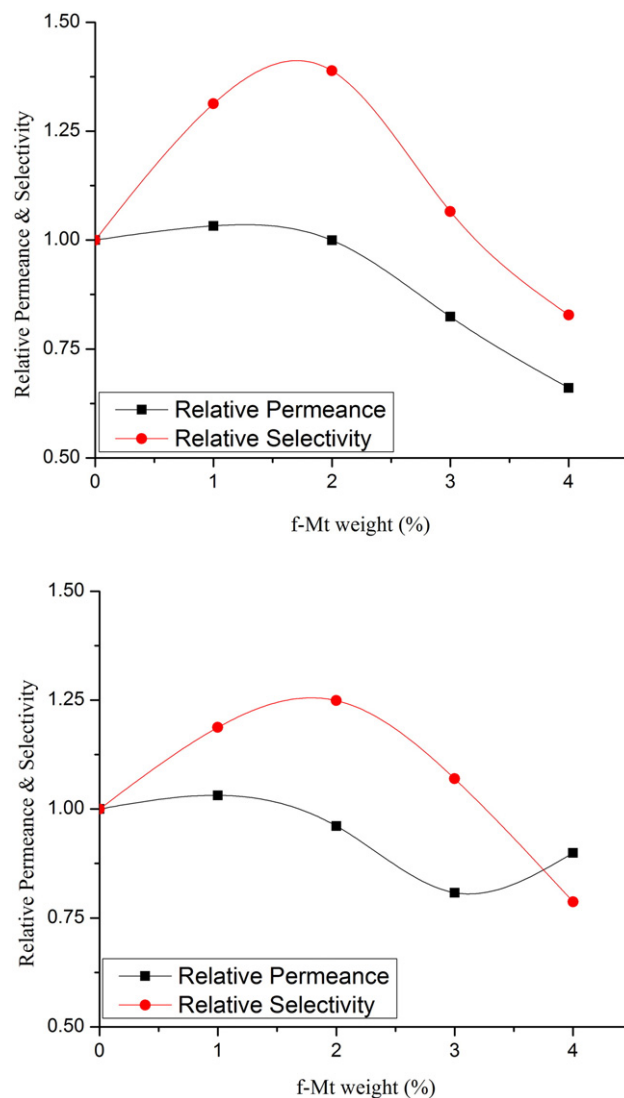

Fig. 6. Effect of *f*-Mt loading on membrane CO_2 permeance and CO_2/CH_4 selectivity at, a) 2 bar (absolute permeance 398.15 GPU & selectivity 1.86), b) 4 bar (absolute permeance 407.01 GPU & selectivity 1.65).
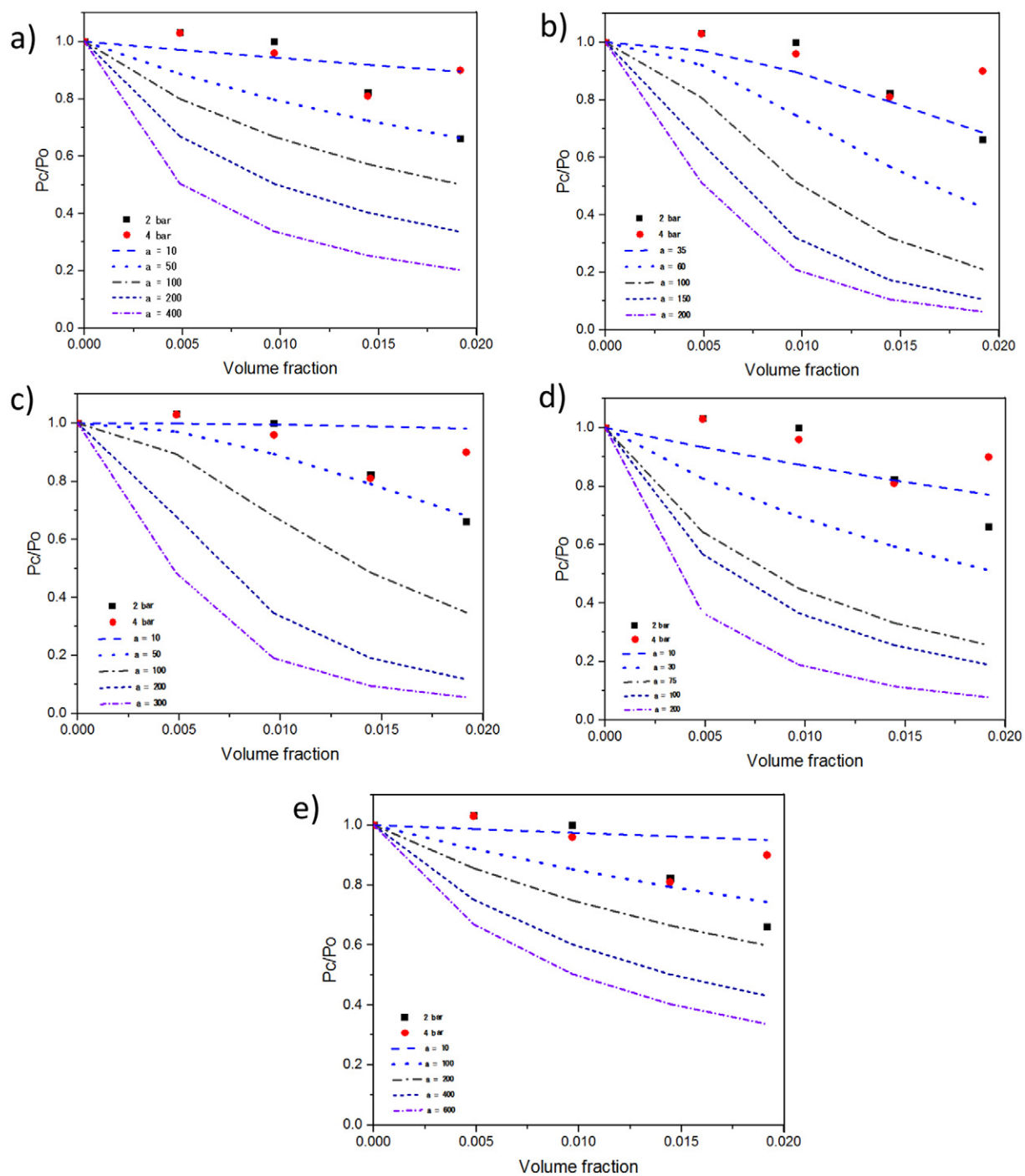
Fig. 7. Relative permeance theoretical curves generated at various aspect ratios (a) from a) Nielsen, (b) Cussler, (c) Yang-Cusssler, (d) Lape-Cussler models, and (e) Bharadwaj models, at 2 and 4 bar for CO_2 gas.

Table 7
Experimental and calculated permeability of CO_2 at 2 bar, aspect ratio and particles per tactoid based of phenomenological models.

Membrane	Model	$P_{r(exp)}$	$P_{r(cal)}$	%AARE	Aspect ratio	No of particles
PEI-f-Mt(1)	Cussler	1.032525	0.9717	−5.88738	35	~4
PEI-f-Mt(2)		0.999447	0.8926	−10.327		
PEI-f-Mt(3)		0.824061	0.7941	−3.63305		
PEI-f-Mt(4)		0.662464	0.6855	3.48481		
PEI-f-Mt(1)	Yang-Cussler	1.032525	0.9712	−5.94164	50	~3
PEI-f-Mt(2)		0.999447	0.8943	−10.5165		
PEI-f-Mt(3)		0.824061	0.7908	−4.03625		
PEI-f-Mt(4)		0.662464	0.6812	2.82495		

particles aspect ratio and volume fraction. In most studies, the average aspect ratio is determined through TEM analysis of the clay mineral layers, followed by permeation estimation through existing models (Yano et al., 1997; Bhole et al., 2007; Picard et al., 2007). However it is also possible to estimate the aspect ratio by inserting the experimental permeation values in the models, where the experimental values are in close agreement to the theoretical values. For instance, Zulhairun and Ismail (2014) prepared psf-cloisite flat sheet membranes and measured the gas permeance values experimentally. These experimental relative permeability values were then used in phenomenological models to estimate the aspect ratio and dispersion state of the dispersed cloisite particles in continuous phase. It can be observed (Fig. 7) that when experimental values are compared to theoretical models, none of the data points fully fit the theoretical curves, nevertheless they follow the same trend at volume fraction above 0.005 for both 2 and 4 bar CO_2 gas pressure. Compared to other models, the Cussler and Yang-Cussler models showed close agreement to the experimental relative permeance. The relative permeance values of CO_2 gas measured through experiments and calculated by theoretical curves generated through Cussler and Yang-Cussler models at aspect ratio 35 and 50 respectively (Table 7). The relative permeance calculated using both models shows very close agreement to experimental relative permeation values. However, at volume fraction 0.19, the relative permeability at 4 bar pressure showed an abrupt increase, which might be due to agglomeration of clay mineral layers at this loading as evident in EDX mapping. The Eq. 4 gives average absolute relative error (%AARE), which is the tuning parameter that describe the close agreement between experimental and calculated values. For better fitting values, the %AARE value should be minimized.

$$\%AARE = \frac{100}{NDP} \sum\nolimits_{J=1}^{NDP} \left| \frac{P_i^{cal} - P_i^{\exp}}{P_i^{\exp}} \right| \qquad (4)$$

where P_i^{cal} and $P_i^{\exp}$ are the relative permeance for the ith experimental value and NDP represents the number of data points. %AARE values varied from −10.52 to +2.82 for Yang-Cussler model, however the maximum value is for 0.01 f-Mt volume fraction whereas all other values for %AARE is approximately ±5. Similar trend of %AARE was found with Cussler model (Table 7).

Bharadwaj (2001) proposed a method to approximate the number of layers of particles in a tactoid through aspect ratio of layered silicate. Yano et al. (1997) studied the water permeability of polyimide-Na-Mt nano-composite and reported the average lateral dimension of Na-Mt as 218 nm. In this study, the number of stakes per unit tactoid is calculated by considering the lateral dimension of Mt as 218 nm with a width of 1 nm, and polymer chains expanded Mt interlayer space to 1 nm. The number of layers per unit tactoid calculated using Yang-Cussler and Cussler models are approximately 3 and 4 respectively. This reflects excellent dispersion properties of f-Mt in PEI matrix. Although, the dispersion state is not fully exfoliated, the particles consist of 3 or 4 layers which is in agreement to literature. From Zulhairun and Ismail's (2014) study on membrane by incorporating filler Cloisite 15A, the number of particles per unit tactoid calculated by phenomenological models ranged from 2 to 4. On the other hand, Kim et al. (2013) prepared AMH-3 cellulose acetate membrane with high shear mixer to delaminate the AMH-3 layered and observed 2–3 particles per unit tactoid for 2–6 wt% AMH-3 loading. In another study, Ismail et al. (2015) prepared PES/Cloisite 15A membrane for CO_2/CH_4 separation, 50% of the tactoids consist of 2–3 particles per unit tactoid for 5 wt% Cloisite 15A loading. Picard et al. (2007) studied the water permeability of Nylon 6-Mt membranes prepared through melt blending process. The average aspect ratio was studied through TEM and STEM analysis and compared through theoretical models which is best fit to the experimental data. The experimental determined average aspect ratio was estimated as 20, whereas Lape-Cussler model give closer value which is 17.2.

At lower volume fraction, the degree of delamination or exfoliation is higher which produced higher aspect ratio or lower number of particles per unit tactoid. Also, the higher f-Mt loading hindered the polymer chains migration in interlayer space. As a result, lower degree of flake delamination took place, however, the relative permeance decrease of membrane is due to reduction in permeable phase. Therefore, from these results, it can be concluded that the modification of Na-MT through aminolauric acid improved the flake dispersion and interaction with PEI matrix.

4. Conclusion

Mixed matrix hollow fibre membranes with various f-Mt loading in PEI matrix were developed via phase inversion method for CO_2/CH_4 separation. The inorganic cations of Na-Mt were replaced with organic cation of aminolauric acid. The modified Mt showed excellent dispersion in the polymer matrix up to 3 wt% f-Mt loading as evident from EDX micrographs. Uniform dispersion of f-Mt enhanced the thermal properties of mixed matrix hollow fibre membrane. FESEM images suggested the uniform finger-like pores throughout the cross section of the spun hollow fibre membranes. The permeation tests were carried out with pure gases at ambient temperature with varying pressures of 2 and 4 bars. An increasing trend in ideal selectivity observed up to 2 wt% f-Mt loading, however opposite trend is observed with increasing filler loading above 2 wt% due to more tortuous path. The maximum ideal selectivity at 2 bar was found with 2 wt% f-Mt loading which showed 39% increment as compared to neat PEI hollow fibre membrane. The increment in selectivity performance is suspected to be related to f-Mt dispersion and aspect ratio in PEI matrix. Cussler and Yang-Cussler models calculated aspect ratio 35 and 50 with 4 and 3 f-Mt particles per unit tactoid respectively. This higher aspect ratio of f-Mt suggested high degree of exfoliation and dispersion which resulted in tortuous factor increment for gas molecules that provide high gas selectivity of PEI-f-Mt membrane.

Acknowledgements

Appendix A. Supplementary data

Supplementary data to this article can be found online at http://dx.doi.org/10.1016/j.clay.2017.03.017.

References

Adame, D., Beall, G.W., 2009. Direct measurement of the constrained polymer region in polyamide/clay nanocomposites and the implications for gas diffusion. Appl. Clay Sci. 42, 545–552.

Anadão, P., Sato, L.F., Wiebeck, H., Valenzuela-Díaz, F.R., 2010. Montmorillonite as a component of polysulfone nanocomposite membranes. Appl. Clay Sci. 48, 127–132.

Bharadwaj, R.K., 2001. Modeling the barrier properties of polymer-layered silicate nanocomposites. Macromolecules 34, 9189–9192.

Bhole, Y.S., Wanjale, S.D., Kharul, U.K., Jog, J.P., 2007. Assessing feasibility of polyarylate–clay nanocomposites towards improvement of gas selectivity. J. Membr. Sci. 306, 277–286.

Choudalakis, G., Gotsis, A.D., 2009. Permeability of polymer/clay nanocomposites: a review. Eur. Polym. J. 45, 967–984.

Chung, T.S., Kafchinski, E.R., Foley, P., 1992. Development of asymmetric hollow fibers from polyimides for air separation. J. Membr. Sci. 75, 181–195.

Chung, T.S., Jiang, L.Y., Li, Y., Kulprathipanja, S., 2007. Mixed matrix membranes (MMMs) comprising organic polymers with dispersed inorganic fillers for gas separation. Prog. Polym. Sci. 32, 483–507.

Cui, Y., Kumar, S., Kona, B.R., van Houcke, D., 2015. Gas barrier properties of polymer/clay nanocomposites. RSC Adv. 5, 63669–63690.

Cussler, E.L., Hughes, S.E., Ward, W.J., Aris, R., 1988. Barrier membranes. J. Membr. Sci. 38, 161–174.

DashtArzhandi, M.R., Ismail, A.F., Matsuura, T., Ng, B.C., Abdullah, M.S., 2015. Fabrication and characterization of porous polyetherimide/montmorillonite hollow fiber mixed

matrix membranes for CO_2 absorption via membrane contactor. Chem. Eng. J. 269, 51–59.

Garg, P., Singh, R.P., Choudhary, V., 2011. Pervaporation separation of organic azeotrope using poly (dimethyl siloxane)/clay nanocomposite membranes. Sep. Purif. Technol. 80, 435–444.

Goh, P.S., Ismail, A.F., Sanip, S.M., Ng, B.C., Aziz, M., 2011. Recent advances of inorganic fillers in mixed matrix membrane for gas separation. Sep. Purif. Technol. 81, 243–264.

Hashemifard, S.A., Ismail, A.F., Matsuura, T., 2011. Effects of montmorillonite nano-clay fillers on PEI mixed matrix membrane for CO_2 removal. Chem. Eng. J. 170, 316–325.

Herrera-Alonso, J.M., Marand, E., Little, J.C., Cox, S.S., 2009. Transport properties in poly-urethane/clay nanocomposites as barrier materials: effect of processing conditions. J. Membr. Sci. 337, 208–214.

Herrera-Alonso, J.M., Sedláková, Z., Marand, E., 2010. Gas transport properties of polyacrylate/clay nanocomposites prepared via emulsion polymerization. J. Membr. Sci. 363, 48–56.

Hsiao, S.H., Liou, G.S., Chang, L.M., 2001. Synthesis and properties of organosoluble poly-imide/clay hybrids. J. Appl. Polym. Sci. 80, 2067–2072.

Husain, S., Koros, W.J., 2009. Macrovoids in hybrid organic/inorganic hollow fiber mem-branes. Ind. Eng. Chem. Res. 48, 2372–2379.

Iman, M., Manhar, A.K., Mandal, M., Maji, T.K., 2014. Preparation and characterization of zinc oxide and nanoclay reinforced crosslinked starch/jute green nanocomposites. RSC Adv. 4, 33826–33839.

Ismail, N.M., Ismail, A.F., Mustafa, A., Matsuura, T., Soga, T., Nagata, K., Asaka, T., 2015. Qualitative and quantitative analysis of intercalated and exfoliated silicate layers in asymmetric polyethersulfone/cloisite15A® mixed matrix membrane for CO_2/CH_4 separation. Chem. Eng. J. 268, 371–383.

Jamil, A., Ching, O.P., Shariff, A., 2014. Polymer-nanoclay mixed matrix membranes for CO_2/CH_4 separation: a review. Appl. Mech. Mater. 625, 690–695.

Jamil, A., Ching, O.P., Shariff, A., 2016a. Current status and future prospect of polymer-layered silicate mixed matrix membranes for CO_2/CH_4 separation. Chem. Eng. Technol. 39, 1393–1405.

Jamil, A., Ching, O.P., Shariff, A., 2016b. Minimizing morphological defects of PEI hollow fibre membrane by optimizing the dope viscosity. APRN J. 11, 1687–1691.

Jiang, L.Y., Chung, T.S., Cao, C., Huang, Z., Kulprathipanja, S., 2005. Fundamental under-standing of nano-sized zeolite distribution in the formation of the mixed matrix single-and dual-layer asymmetric hollow fiber membranes. J. Membr. Sci. 252, 89–100.

Khayet, M., 2003. The effects of air gap length on the internal and external morphology of hollow fiber membranes. Chem. Eng. Sci. 58, 3091–3104.

Kim, G.M., Lee, D.H., Hoffmann, B., Kressler, J., Stöppelmann, G., 2001. Influence of nanofillers on the deformation process in layered silicate/polyamide-12 nanocom-posites. Polymer 42, 1095–1100.

Kim, Y.K., Park, H.B., Lee, Y.M., 2005. Preparation and characterization of carbon molecular sieve membranes derived from BTDA–ODA polyimide and their gas separation prop-erties. J. Membr. Sci. 255, 265–273.

Kim, W.G., Lee, J.S., Bucknall, D.G., Koros, W.J., Nair, S., 2013. Nanoporous layered silicate AMH-3/cellulose acetate nanocomposite membranes for gas separations. J. Membr. Sci. 441, 129–136.

Lape, N.K., Nuxoll, E.E., Cussler, E.L., 2004. Polydisperse flakes in barrier films. J. Membr. Sci. 236, 29–37.

Liang, C.Y., Uchytil, P., Petrychkovych, R., Lai, Y.C., Friess, K., Sipek, M., Reddy, M.M., Suen, S.Y., 2012. A comparison on gas separation between PES/MMT and PES/TiO_2 mixed matrix membranes. Sep. Purif. Technol. 92, 57–63.

Mittal, V., 2009. Polymer layered silicate nanocomposites: a review. Materials 2, 992–1057.

Nassar, N., Utracki, L.A., Kamal, M.R., 2005. Melt intercalation in montmorillonite/polysty-rene nanocomposites. Int. Polym. Process. 20, 423–431.

Nielsen, L.E., 1967. Models for the permeability of filled polymer systems. J. Macromol. Sci. Chem. 1, 929–942.

Okada, A., Usuki, A., 1995. The chemistry of polymer-clay hybrids. Mater. Sci. Eng. C 3, 109–115.

Pavlidou, S., Papaspyrides, C.D., 2008. A review on polymer–layered silicate nanocompos-ites. Prog. Polym. Sci. 33, 1119–1198.

Picard, E., Vermogen, A., Gérard, J.F., Espuche, E., 2007. Barrier properties of nylon 6-montmorillonite nanocomposite membranes prepared by melt blending: influence of the clay content and dispersion state: consequences on modelling. J. Membr. Sci. 292, 133–144.

Ren, J., Li, Z., Wong, F.S., 2004. Membrane structure control of BTDA-TDI/MDI (P84) co-polyimide asymmetric membranes by wet-phase inversion process. J. Membr. Sci. 241, 305–314.

Rezaei, M., Ismail, A.F., Hashemifard, S.A., Matsuura, T., 2014. Preparation and characteri-zation of PVDF-montmorillonite mixed matrix hollow fiber membrane for gas–liquid contacting process. Chem. Eng. Res. Des. 92, 2449–2460.

Rubio, C., Zornoza, B., Gorgojo, P., Tellez, C., Coronas, J., 2014. Separation of H_2 and CO_2 containing mixtures with mixed matrix membranes based on layered materials. Curr. Org. Chem. 18, 2351–2363.

Takahashi, N., Kuroda, K., 2011. Materials design of layered silicates through covalent modification of interlayer surfaces. J. Mater. Chem. 21, 14336–14353.

Tan, B., Thomas, N.L., 2016. A review of the water barrier properties of polymer/clay and polymer/graphene nanocomposites. J. Membr. Sci. 514, 595–612.

Uddin, F., 2008. Clays, nanoclays, and montmorillonite minerals. Metall. Mater. Trans. A 39, 2804–2814.

Wang, D., Teo, W.K., Li, K., 2002. Preparation and characterization of high-flux polysulfone hollow fibre gas separation membranes. J. Membr. Sci. 204, 247–256.

Yampolskii, Y., 2012. Polymeric gas separation membranes. Macromolecules 45, 3298–3311.

Yang, C., Smyrl, W.H., Cussler, E.L., 2004. Flake alignment in composite coatings. J. Membr. Sci. 231, 1–12.

Yano, K., Usuki, A., Okada, A., 1997. Synthesis and properties of polyimide-clay hybrid films. J. Polym. Sci. A Polym. Chem. 35, 2289–2294.

Zanetti, M., Lomakin, S., Camino, G., 2000. Polymer layered silicate nanocomposites. Macromol. Mater. Eng. 279, 1–9.

Zhou, L., Chen, H., Jiang, X., Lu, F., Zhou, Y., Yin, W., Ji, X., 2009. Modification of montmo-rillonite surfaces using a novel class of cationic gemini surfactants. J. Colloid Interface Sci. 332, 6–21.

Zulhairun, A.K., Ismail, A.F., 2014. The role of layered silicate loadings and their dispersion states on the gas separation performance of mixed matrix membrane. J. Membr. Sci. 468, 20–30.

Zulhairun, A.K., Ismail, A.F., Matsuura, T., Abdullah, M.S., Mustafa, A., 2014. Asymmetric mixed matrix membrane incorporating organically modified clay particle for gas sep-aration. Chem. Eng. J. 241, 495–503.